INTERNATIONAL JOURNAL FOR NUMERICAL METHODS IN FLUIDS
Int. J. Numer. Meth. Fluids 2004; **45**:441–461 (DOI: 10.1002/fld.707)

An aeroacoustic hybrid approach for non-isothermal flows at low Mach number

F. Golanski[1], C. Prax[1,*,†], E. Lamballais[1], V. Fortuné[2] and J.-C. Valière[1]

[1]*Laboratoire d'Etudes Aérodynamiques, Université de Poitiers, Bât. K.-40, avenue du Recteur Pineau, 86022 Poitiers Cedex, France*
[2]*Institut de Mécanique des Fluides, Institut National Polytechnique, Allée Camille Soula, 31400 Toulouse, France*

SUMMARY

This paper presents an aeroacoustic hybrid technique for the study of non-isothermal flows at low Mach number. The flow dynamics and the acoustic production and propagation are computed separately. The fully compressible Navier–Stokes equations are modified through an expansion of the physical quantities using a low Mach number approximation. Compressibility effects are thus removed in the CFD while inhomogeneities of the flow related to heat transfer are preserved. One advantage is a reduction of the time step constraint. Another advantage is that the Mach number does not appear explicitly and a simple rescaling allows a study over a relatively wide band of subsonic Mach number flows with a single dynamic simulation.

Compatible acoustic source terms for LEE based propagation have been defined and the procedure is implemented in the case of a temporal mixing layer. Compressible simulations for Mach numbers of 0.2, 0.3 and 0.4 are compared with the numerical results obtained using the proposed method. Very good agreement is obtained even at relatively high subsonic Mach number demonstrating the efficiency of the proposed technique. Copyright © 2004 John Wiley & Sons, Ltd.

KEY WORDS: low Mach number; source terms; aeroacoustics; linearized Euler's equations; non-isothermal flow

1. INTRODUCTION

The increased performance of computers in the last decade has led to the development of very accurate numerical methods in the scientific field. In computational aeroacoustics, the direct numerical simulation (DNS)—which consists in the resolution of the whole aeroacoustic problem with the consideration of all the scales that occur in the flow—is now accessible.

However, in the case of low Mach number flows, DNS remains very expensive in terms of computational time. Indeed, in this case, the time step is imposed by the sound velocity,

*Correspondence to: C. Prax, Laboratoire d'Etudes Aérodynamiques, UMR CNRS 6609, Université de Poitiers, Bât. K.-40, avenue du Recteur Pineau, 86022 Poitiers Cedex, France.
†E-mail: christian.prax@lea.univ-poitiers.fr

Received 24 February 2003
Revised 18 August 2003

whereas the pressure fluctuations associated with acoustic phenomena are typically three to five orders of magnitude smaller than pressure fluctuations associated with turbulent events. So, in this situation, a very wide range of scales have to be accurately simulated, leading to very expensive simulations. Consequently, DNS in Computational Aero-Acoustics (CAA) can only be used for a small number of academic problems, which nevertheless provide data of great interest for the understanding of physical phenomena.

More efficient methods are thus required for industrial applications. In this context, a great deal of research has been devoted to the development of hybrid methods. The hybrid methods consist in considering the different physical phenomena separately in order to choose the most efficient numerical tool for each.

This type of methods was initiated by Lighthill [1, 2]. His famous analogy separates the problems of the sound generation by the unsteady flows from those of the sound propagation. In this method, the local flow field is used to determine the acoustic source terms that are introduced at a second step in the propagation equation solved to obtain the acoustic far-field. Lighthill's analogy proved to be an efficient tool and a great number of work has since been developed to the improvement of this type of approach. In particular, Lighthill's analogy is not able to correctly describe the effects of the flow on the propagation of acoustic waves. A number of analogies have thus been studied to spread the domain of application of hybrid methods.

Among these approaches is the Phillips [3] equation which allows the effects of a moving media with non-uniform sound speed to be included. A more complete third-order propagation equation was defined by Lilley [4], including the effects of refraction and convection by the flow. But this equation poses difficulties related to its integration, leading to a limited use.

On the other hand, the Linearized Euler's Equations (LEE) are written as a set of partial differential equations. A Green's function is thus not required for their resolution and their use in geometrically complex problems is more accessible than other analogies. Moreover, the LEE are capable of a good description of the convection and refraction effects of a non-uniform flow.

A crucial point in such a method is the determination of the acoustic source terms. These source terms are extracted from a CFD simulation which can be a large Eddy simulation (LES) [5–7], a DNS (compressible or incompressible) or a Reynolds Averaged Navier–Stokes simulation (RANS) [8, 9]. In the case of flow evolving at low Mach number, the incompressible DNS is much less expensive than the compressible DNS, thanks to the absence of acoustic phenomena. A hybrid method composed of an incompressible DNS coupled to a LEE simulation is thus less expensive than an aeroacoustic DNS [10]. A major disadvantage of this technique is that the classical incompressible Navier–Stokes equations cannot be used in the case of non-isothermal flows [11, 12]. In such a situation, a low Mach number approximation (LMNA), which can be assimilated to a quasi-incompressible approximation, first developed in the frame of low Mach number reacting flows, can be used. Indeed, DNS of low Mach number reacting flows is quite difficult on account of the presence of acoustic phenomena which are very much faster than chemical reactions whereas their effects on the different physical events are often negligible. For such computations, a set of equations derived from the fully compressible Navier–Stokes equations has been developed so that inhomogeneities of the flow (in term of density fluctuations) related to heat transfer are well described, whereas compressibility effects (like the presence of acoustic waves) are removed [11–13].

Several acoustic/flow decomposition based on different physical or numerical analysis of the problem [14–16] can be found in the literature.

The hybrid method presented in this study is constituted of a quasi-incompressible DNS (called LMNA in this paper) and the LEE. This paper can be considered as a validation step of the formulation of the acoustic source terms determined by a LMNA in the case of non-isothermal flows.

The second part of the paper is dedicated to the presentation of the low Mach number approximation. In the third section, developments and suitable assumptions which lead to the acoustic equations and source terms are presented. The fourth part describes the flow configuration chosen as a test case, and the numerical methodologies used in the different codes. Isothermal and non-isothermal simulations are computed and compared to compressible DNS results as references. Conclusions are finally presented concerning the validity, efficiency and the advantages of the present approach.

2. THE LOW MACH NUMBER APPROXIMATION

This part is dedicated to the description of the equations used in the CFD code.

Throughout the paper, all dimensional variables are denoted by the superscript *.

The equations of the low Mach number approximation (LMNA) used in this work are deduced [11, 12] from the compressible Navier–Stokes equations for a perfect-gas which are written in conservative non-dimensional form

$$\frac{\partial \rho}{\partial t} + \frac{\partial \rho u_j}{\partial x_j} = 0 \tag{1}$$

$$\frac{\partial \rho u_i}{\partial t} + \frac{\partial \rho u_i u_j}{\partial x_j} = -\frac{\partial p}{\partial x_i} + \frac{1}{Re}\frac{\partial \tau_{ij}}{\partial x_j} \tag{2}$$

$$\frac{\partial E}{\partial t} + \frac{\partial (p+E)u_j}{\partial x_j} = \frac{1}{Re}\frac{\partial u_i \tau_{ij}}{\partial x_j} + \frac{1}{M^2 Re\, Pr(\gamma-1)}\frac{\partial^2 T}{\partial x_j^2} \tag{3}$$

$$p = \frac{\rho T}{\gamma M^2} \tag{4}$$

in Cartesian co-ordinates $x_i = (x, y, z)$, where $u_i = (u, v, w)$ are the velocity components, (p, ρ, T) are respectively the pressure, the density and the temperature fields. E is the total energy per unit volume and τ_{ij} is the viscous stress tensor, given respectively by

$$E = \frac{p}{\gamma - 1} + \frac{1}{2}\rho u_i u_i \tag{5}$$

and

$$\tau_{ij} = \frac{\partial u_i}{\partial x_j} + \frac{\partial u_j}{\partial x_i} - \frac{2}{3}\frac{\partial u_k}{\partial x_k}\delta_{ij} \tag{6}$$

All variables have been non-dimensionalised using L^*_{ref}, U^*_{ref}, ρ^*_{ref}, T^*_{ref}, and $t^*_{\text{ref}} = L^*_{\text{ref}}/U^*_{\text{ref}}$ as references length, velocity, density, temperature and time. $\gamma = c^*_p/c^*_v$ is the ratio of specific heats and the universal gas constant is $r^* = c^*_p - c^*_v$. The three fundamental non-dimensional parameters are the Reynolds number $Re = \rho^*_{\text{ref}} U^*_{\text{ref}} L^*_{\text{ref}}/\mu^*$, the Prandtl number $Pr = \mu^* c^*_p/k^*$, and the Mach number $M = U^*_{\text{ref}}/\sqrt{\gamma r^* T^*_{\text{ref}}}$.

The low Mach number approximation [11, 12], is obtained from (1)–(4) by expanding all the variables of the flow in power series in $\varepsilon = \gamma M^2$. These expansions are expressed as follows

$$\rho = \rho^{(0)} + \varepsilon\rho^{(1)} + \cdots \tag{7}$$

$$u_i = u_i^{(0)} + \varepsilon u_i^{(1)} + \cdots \tag{8}$$

$$T = T^{(0)} + \varepsilon T^{(1)} + \cdots \tag{9}$$

while the equation of state (4) imposes an expansion for p such that

$$p = \frac{p^{(0)}}{\varepsilon} + p^{(1)} + \cdots \tag{10}$$

In Equation (10), $p^{(0)}$ and $p^{(1)}$ can be interpreted, as it is done in References [11, 12], respectively as a thermodynamic pressure and a fluid dynamic pressure.

By substituting (7)–(10) into Equations (1)–(4), the lowest order in ε leads to

$$\frac{\partial\rho^{(0)}}{\partial t} + \frac{\partial\rho^{(0)}u_i^{(0)}}{\partial x_i} = 0 \tag{11}$$

$$\frac{\partial p^{(0)}}{\partial x_i} = 0 \tag{12}$$

$$\rho^{(0)}\frac{\partial u_j^{(0)}}{\partial x_j} = \frac{1}{Re\,Pr\,T^{(0)}}\frac{\partial^2 T^{(0)}}{\partial x_j^2} \tag{13}$$

$$p^{(0)} = \rho^{(0)} T^{(0)} \tag{14}$$

According to (12), the thermodynamic pressure $p^{(0)}$ is spatially uniform. Since an open physical domain is considered here, $p^{(0)}$ is also assumed to be constant in time.

In order to close the system, an additional equation is required, so equation (2) is considered for the zeroth-order in ε:

$$\frac{\partial\rho^{(0)}u_i^{(0)}}{\partial t} + \frac{\partial\rho^{(0)}u_i^{(0)}u_j^{(0)}}{\partial x_j} = -\frac{\partial p^{(1)}}{\partial x_i} + \frac{1}{Re}\frac{\partial\tau_{ij}^{(0)}}{\partial x_j} \tag{15}$$

Finally the governing dynamical equations are (11), (13), (14) and (15). Details of the numerical resolution of these equations can be found in References [11, 12]. It is important to emphasize that these equations are only valid for a vanishing Mach number, but there is no restriction where the spatiotemporal density variations are concerned. In fact, the Mach number does not appear in a CFD simulation based on LMNA, but an appropriate rescaling

of the results of such a simulation allows predictions corresponding to flows evolving at different Mach numbers. Obviously, the restriction of this last point is the validity limit of any incompressible assumption.

3. FROM LMNA TO ACOUSTICS

Starting from the CFD model for non-isothermal low Mach number flows, a new step consists now in restoring acoustic motion, in order to lead to an effective hybrid method. The process consists in deriving the acoustics from the decomposition used to get the flow dynamics using appropriate assumptions, and bringing to the fore the propagation equations with suitable source terms.

In the LMNA decomposition presented in the previous part, the fully compressible Navier–Stokes equations have been decomposed at the lowest order in ε. Now, since we are interested in acoustic variables, we will focus our attention on the upper order of the compressible equations

$$\frac{\partial \rho^{(1)}}{\partial t} + \frac{\partial}{\partial x_j}(\rho^{(0)} u_j^{(1)} + \rho^{(1)} u_j^{(0)}) = 0 \tag{16}$$

$$\frac{\partial \rho^{(0)} u_i^{(1)}}{\partial t} + \rho^{(1)} \frac{\partial u_i^{(0)}}{\partial t} + (\rho^{(0)} u_j^{(1)} + \rho^{(1)} u_j^{(0)}) \frac{\partial u_i^{(0)}}{\partial x_j} + \frac{\partial \rho^{(0)} u_j^{(0)} u_i^{(1)}}{\partial x_j} = \frac{1}{Re} \frac{\partial \tau_{ij}^{(1)}}{\partial x_j} \tag{17}$$

$$\frac{\partial p^{(1)}}{\partial t} + \frac{\partial}{\partial x_j}(p^{(1)} u_j^{(0)} + \gamma p^{(0)} u_j^{(1)}) + (\gamma - 1) p^{(1)} \frac{\partial u_j^{(0)}}{\partial x_j} = \frac{\gamma - 1}{Re} \tau_{kj}^{(0)} \frac{\partial u_k^{(0)}}{\partial x_j} + \frac{\gamma}{Re\, Pr} \frac{\partial^2 T^{(1)}}{\partial x_j^2} \tag{18}$$

In the frame of acoustic waves traveling along a short distance, the propagation features are hardly affected by viscous effects. Moreover, Lighthill [1, 2] showed that for free subsonic flows at sufficiently high Reynolds number, viscous noise can be neglected with respect to shear noise. Then, the viscous terms of (16)–(18)—$(1/Re)\partial \tau_{ij}^{(1)}/\partial x_j$ in (17), and

$$\frac{\gamma - 1}{Re} \tau_{kj}^{(0)} \frac{\partial u_k^{(0)}}{\partial x_j} + \frac{\gamma}{Re\, Pr} \frac{\partial^2 T^{(1)}}{\partial x_j^2}$$

in (18)—can be neglected, and the following system is obtained:

$$\frac{\partial \rho^{(1)}}{\partial t} + \frac{\partial}{\partial x_j}(\rho^{(0)} u_j^{(1)} + \rho^{(1)} u_j^{(0)}) = 0 \tag{19}$$

$$\frac{\partial \rho^{(0)} u_i^{(1)}}{\partial t} + \rho^{(1)} \frac{\partial u_i^{(0)}}{\partial t} + (\rho^{(0)} u_j^{(1)} + \rho^{(1)} u_j^{(0)}) \frac{\partial u_i^{(0)}}{\partial x_j} + \frac{\partial \rho^{(0)} u_j^{(0)} u_i^{(1)}}{\partial x_j} = 0 \tag{20}$$

$$\frac{\partial p^{(1)}}{\partial t} + \frac{\partial}{\partial x_j}(p^{(1)} u_j^{(0)} + \gamma p^{(0)} u_j^{(1)}) + (\gamma - 1) p^{(1)} \frac{\partial u_j^{(0)}}{\partial x_j} = 0 \tag{21}$$

At this stage, one almost recognizes the linearized Euler's equations. Nevertheless, there are still three differences with the LEE generally used. The first is the presence of $\rho^{(1)}(\partial u_i^{(0)}/\partial t)$ in (19). In the literature, the LEE are often solved by considering the propagation over a steady mean flow. In that case, this term can be dropped. The treatment of the mean flow will be discussed in detail in Section 4.3. Secondly, contrary to (20), the equation of the LEE concerning the energy conservation contains the term $-(\gamma-1)u_j^{(1)}\partial p^{(0)}/\partial x_j$. However, Equation (12) shows that $\partial p^{(0)}/\partial x_i$ is zero for all i. A third difference between (18)–(20) and the LEE is the lack of pressure gradient $\partial p^{(1)}/\partial x_i$ in (19). Then, modifying (19) by adding $\partial p^{(1)}/\partial x_i$ in the LHS and the RHS gives

$$\frac{\partial \rho^{(0)}u_i^{(1)}}{\partial t}+(\rho^{(0)}u_j^{(1)}+\rho^{(1)}u_j^{(0)})\frac{\partial u_i^{(0)}}{\partial x_j}+\frac{\partial \rho^{(0)}u_j^{(0)}u_i^{(1)}}{\partial x_j}+\frac{\partial p^{(1)}}{\partial x_i}=\frac{\partial p^{(1)}}{\partial x_i} \tag{22}$$

This last trick of arithmetic allows the left hand side of Equations (18)–(21) to be identified as the classical LEE for a small perturbation $(p^{(1)},u_i^{(1)},\rho^{(1)})$ over a steady mean flow $(p^{(0)},u_i^{(0)},\rho^{(0)})$. Now, Equation (21) differs from LEE momentum equation by a forcing term in the RHS, which defines the flow generated noise.

At this stage, the meaning of $p^{(1)}$ in the LHS and the RHS must be discussed. Indeed, the LEE are likely to support acoustic, vorticity and entropy wave modes. The presence of each of these modes in the computed solution depends only on the nature of the forcing term employed. So $p^{(1)}$ in the LHS can contain both acoustic and vorticity fluctuations (and so must results on solving LEE). On the other hand, the forcing term must be provided and evaluated by the solution of the CFD simulation (in which the acoustics are absent). So $p^{(1)}$ (RHS) will involve only aerodynamic fluctuations. The LMNA leads to this term being expressed using Equation (15), in which viscous effects are neglected [1, 2].

As the vorticity mode is convected by the flow, it stays confined to the CFD zone. In that region, acoustical and fluid dynamic fluctuations cannot be separated. The acoustic mode will propagate beyond and a more extended computational grid can be employed for the solution of LEE so as to extract the acoustics.

Finally, the acoustic production and propagation can be obtained by solving the following equations:

$$\frac{\partial \rho^{(1)}}{\partial t}+\frac{\partial}{\partial x_j}(\rho^{(0)}u_j^{(1)}+\rho^{(1)}u_j^{(0)})=0 \tag{23}$$

$$\frac{\partial \rho^{(0)}u_i^{(1)}}{\partial t}+(\rho^{(0)}u_j^{(1)}+\rho^{(1)}u_j^{(0)})\frac{\partial u_i^{(0)}}{\partial x_j}+\frac{\partial \rho^{(0)}u_j^{(0)}u_i^{(1)}}{\partial x_j}+\frac{\partial p^{(1)}}{\partial x_i}=S_i \tag{24}$$

$$\frac{\partial p^{(1)}}{\partial t}+\frac{\partial}{\partial x_j}(p^{(1)}u_j^{(0)}+\gamma p^{(0)}u_j^{(1)})+(\gamma-1)p^{(1)}\frac{\partial u_j^{(0)}}{\partial x_j}=0 \tag{25}$$

where S_i stands for the acoustic source term

$$S_i=-\left[\frac{\partial \rho^{(0)}u_i^{(0)}}{\partial t}+\frac{\partial \rho^{(0)}u_i^{(0)}u_j^{(0)}}{\partial x_j}\right] \tag{26}$$

This source term is consistent with the one defined in References [5, 14]. Indeed, the divergence of

$$\frac{\partial \rho^{(0)} u_i^{(0)}}{\partial t} \tag{27}$$

is equal to zero in the isothermal case, so it does not excite the acoustic mode. In isothermal case, (25) thus reduces to

$$\frac{\partial \rho^{(0)} u_i^{(0)} u_j^{(0)}}{\partial x_j} \tag{28}$$

which corresponds to the velocity fluctuations in the flow. This term, which is the same as that defined in References [5, 7] contains the shear noise and the self noise and is sufficient for isothermal flows.

In the non-isothermal case, (27) is not divergence-free, so it acts as an additional acoustic source. The entire form (25) of S_i is then required. The term (26) involves temporal fluctuations of momentum in the flow, in the case where the density distribution is not homogeneous. The density inhomogeneities create different accelerations between neighbouring particles in the turbulent zone [17]. Equation (15), in which viscous effects are neglected, can be rewritten as

$$\frac{Du_i^{(0)}}{Dt} + \frac{u_i^{(0)}}{\rho^{(0)}} \frac{D\rho^{(0)}}{Dt} = -\frac{1}{\rho^{(0)}} \frac{\partial p^{(1)}}{\partial x_i} \tag{29}$$

where

$$\frac{D\cdot}{Dt} = \frac{\partial \cdot}{\partial t} + u_i^{(0)} \frac{\partial \cdot}{\partial x_i}$$

Compared to the isothermal case in which

$$\frac{Du_i^{(0)}}{Dt} = -\frac{1}{\rho^{(0)}} \frac{\partial p^{(1)}}{\partial x_i} \tag{30}$$

the pressure fluctuations of the non-isothermal case are governed by the same acceleration fluctuations $Du_i^{(0)}/Dt$ supplemented by fluctuations due to density inhomogeneities

$$\frac{u_i^{(0)}}{\rho^{(0)}} \frac{D\rho^{(0)}}{Dt}$$

4. TEST CASES: ISOTHERMAL AND NON-ISOTHERMAL TEMPORAL MIXING LAYER

4.1. Flow configuration

The temporally evolving mixing layer has been chosen to validate the modeling of the acoustic source terms. This test-case has been used in several numerical works in fluid dynamics [18–20], and in aeroacoustics [21, 22].

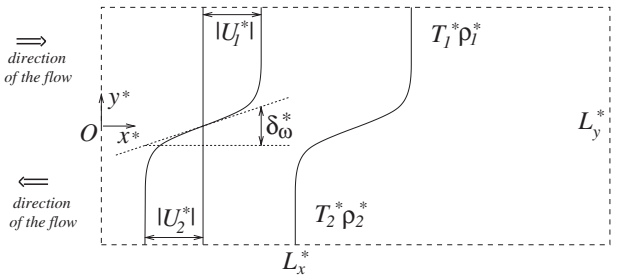

Figure 1. The temporal mixing layer flow configuration.

This flow is studied in a rectangular numerical domain ($L_x^* \times L_y^*$) between two streams of different velocities, temperatures and densities, respectively denoted (U_1^*, T_1^*, ρ_1^*) in the upper half domain and (U_2^*, T_2^*, ρ_2^*) in the lower half. The notation is shown in Figure 1.

In this application, the references are $L_{\text{ref}}^* = \delta_\omega^*$ (where δ_ω^* is the initial vorticity thickness), $U_{\text{ref}}^* = U_1^* - U_2^*$, $T_{\text{ref}}^* = T_2^*$ and $\rho_{\text{ref}}^* = \rho_2^*$. The Reynolds and Prandtl numbers are taken as $Re = 400$ and $Pr = 0.75$. It has been shown in Reference [21] that viscosity effects in the acoustic sources are negligible in the present configuration even at this moderate Reynolds number. The initial pressure p^* is assumed to be uniform. The initial mean velocity field is given by the following hyperbolic-tangent profile

$$\langle u^* \rangle (y^*) = \frac{U_1^* + U_2^*}{2} + \frac{U_1^* - U_2^*}{2} \tanh\left(\frac{2y^*}{\delta_\omega^*}\right) \tag{31}$$

The initial temperature field is deduced using the Crocco–Buseman relation

$$T^*(y^*) = \frac{1}{2c_p^*}\left[-\langle u^* \rangle^2 (y^*) - U_1^* U_2^* + \langle u^* \rangle (y^*)(U_1^* + U_2^*)\right]$$
$$+ (T_1^* - T_2^*)\frac{\langle u^* \rangle (y^*)}{U_1^* - U_2^*} + \frac{T_2^* U_1^* - T_1^* U_2^*}{U_1^* - U_2^*} \tag{32}$$

where the $\langle . \rangle$ operator is the mean value over the periodic direction:

$$\langle \alpha \rangle (y,t) = \frac{1}{L_x}\int_0^{L_x} \alpha(x,y,t)\,\mathrm{d}x \tag{33}$$

The flow is perturbed using an incompressible disturbance field ($\tilde{u}^*, \tilde{v}^*$) composed of a fundamental and two sub-harmonic disturbances.

The choice of this somewhat specific flow has been motivated by several arguments. First, it is worth keeping in mind that the present work is a validation step in the domain of hybrid approaches in CAA. In this context, the temporal mixing layer, although being an academic configuration, exhibits a lot of advantages. Firstly, the mixing layer is a fundamental flow greatly studied in the literature. Secondly, the temporal flow has physical properties which allow numerical difficulties like the evacuation of acoustic and vorticity modes at the outflow and inflow boundaries to be avoided. Lastly, the numerical domain can be smaller than that used in a spatial configuration: such a validation is thus less expensive in

computational time and memory requirements. Other temporal flows has been studied in CAA as in Reference [23].

In a first step, an isothermal test, for which the acoustical source terms are now well known [5, 7, 14], is computed to confirm that the temporal mixing layer can be used as a benchmark in the validation of a CAA code. The results provided by the hybrid method are compared to compressible DNS simulations. By definition, the DNS of the compressible Navier–Stokes equations consists in the solving of the CAA problem without any supplementary modeling. So, the compressible DNS results are considered in this work as reference. Moreover, the initial conditions used in the LMNA simulation correspond exactly to those used in the compressible one, allowing direct comparisons of the different simulations.

The non-isothermal configuration is simulated in a second step to validate the LMNA/LEE procedure using the acoustic source terms defined by Equation (25).

4.2. Numerical implementation

The flow and acoustic computations are performed on Cartesian grids. However, for information, the LMNA solver uses the sixth-order compact finite difference scheme of Reference [24] to compute spatial derivatives, and a third-order Runge–Kutta scheme for time integration. The flow is assumed to be periodic in the streamwise direction, while a free-slip boundary condition is used for $y^* = \pm L_y^*/2$.

For the LEE code, the same spatial derivative scheme, and a fourth-order Runge–Kutta scheme are employed. Different schemes are used in the CFD and acoustic parts because the numerical resolution of the LMNA requires, as in an incompressible simulation, the inversion of a Poisson equation for the pressure. The Poisson equation contains, unlike the incompressible model, a term which must be interpolated. This interpolation can modify the global temporal integration order. The use of a temporal interpolation on the subtime steps of a RK4 scheme, even with a high order interpolation scheme, has been found to be less efficient than with a RK3 scheme. The global scheme (Runge–Kutta and interpolation) thus obtained is second order with the third-order Runge–Kutta scheme whereas only first order has been obtained with the fourth-order Runge–Kutta scheme. The resolution of the dynamic problem is not within the scope of this paper, so the numerical methodology employed in the dynamic part will not be discussed in detail. More information can be found in Reference [25] and in a paper under review.

The temporal approximation of the source term (26) is performed by the third-order explicit approximation

$$\left(\frac{\partial f}{\partial t}\right)_n = \frac{1}{\Delta t}\left[\frac{11}{6} f_n - 3 f_{n-1} + \frac{3}{2} f_{n-2} - \frac{1}{3} f_{n-3}\right] \tag{34}$$

The boundary condition in the streamwise direction is also periodic while a non-reflecting boundary condition (NRBC) must be employed in the other direction. An interesting property of the temporal mixing layer [22] is that acoustic waves propagate mainly in the y-direction in the acoustic far-field. This property has already been used to simplify the resolution of the Lighthill's analogy in References [21, 23]. A one-dimensional NRBC can then be employed. Here the one-dimensional characteristic based boundary condition proposed in Reference [26] is used. This condition proved its efficiency in this configuration for the compressible DNS simulation taken as Reference [21].

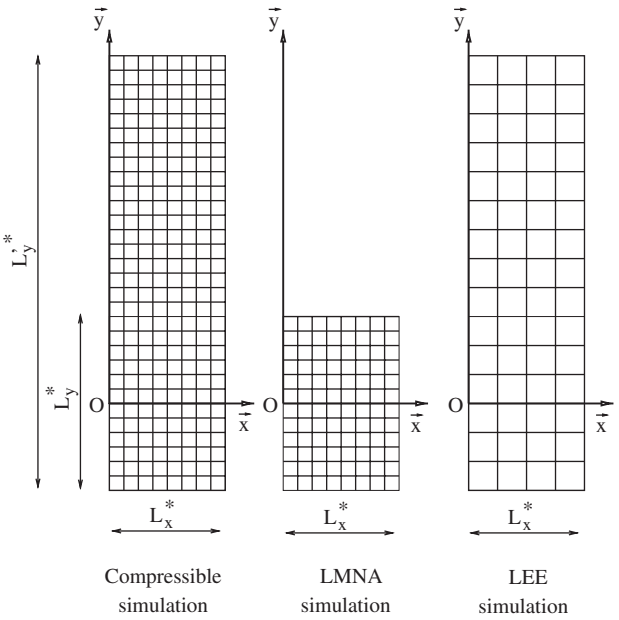

Figure 2. Representation of the different computational grids.

The main advantage of an hybrid method is the reduction of the computational cost. But, to obtain this advantage, the grid resolution of the LEE code must be coarser than that of the dynamic simulation. The time step must also be larger. So an interpolation step must be performed to fit the data of the dynamic simulation to the LEE spatial and temporal grids. For the present simulations, only one out of two points of the LMNA grid are kept for the LEE grid and a cubic spline interpolation is performed to fit the time evolutions. The cubic spline interpolation, by its non-locality, provides a good smoothness for the function obtained, and ensures the continuity of its first two derivatives. Moreover, and it is a decisive property in CAA, this interpolation method generates very few spurious waves [27].

Moreover, the acoustic far-field must be computed in a region where there are no aerodynamic sources. The physical domain of the LEE simulation is thus chosen larger than the LMNA simulation. In order to make comparisons of the results, the compressible simulation is extended to the whole LEE physical domain. Figure 2 schematically shows the characteristics of the different grids. The spatial decimation of the data provided by the LMNA code introduces some spurious waves in the LEE computation. As these waves are not correctly evacuated by the boundary conditions, a spatial filtering (the six-order compact filter of Reference [24]) is applied.

4.3. Mean flow

In other studies using the LEE [5, 7], the mean flow of the acoustic simulation is deduced from LES data by taking the mean value of the dynamic quantities over a period corresponding

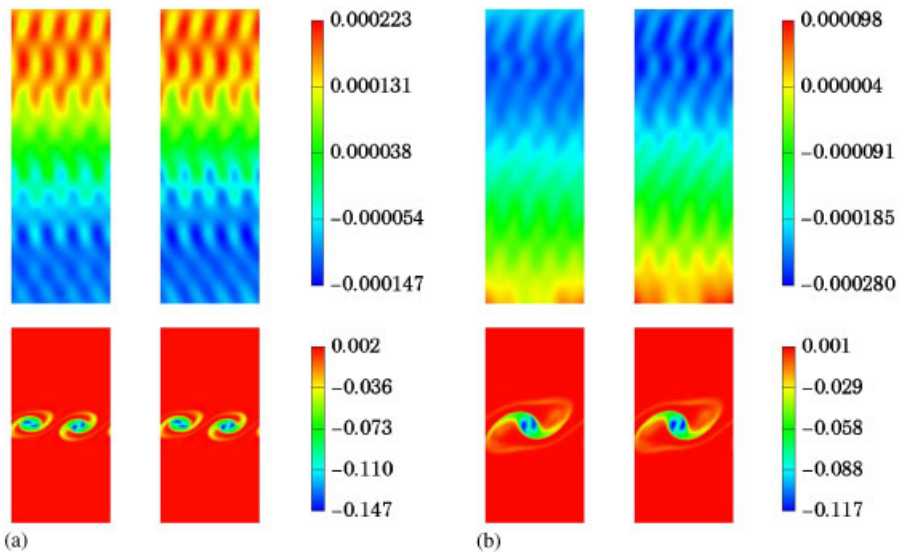

Plate 1. Isothermal case. Instantaneous fields at: (a) t=53.6, (b) $t = 14.6$ for $M = 0.2$. Top: Instantaneous acoustic density fields in the acoustic region. Bottom: Instantaneous vorticity fields in the source region. Compressible simulation is at the left.

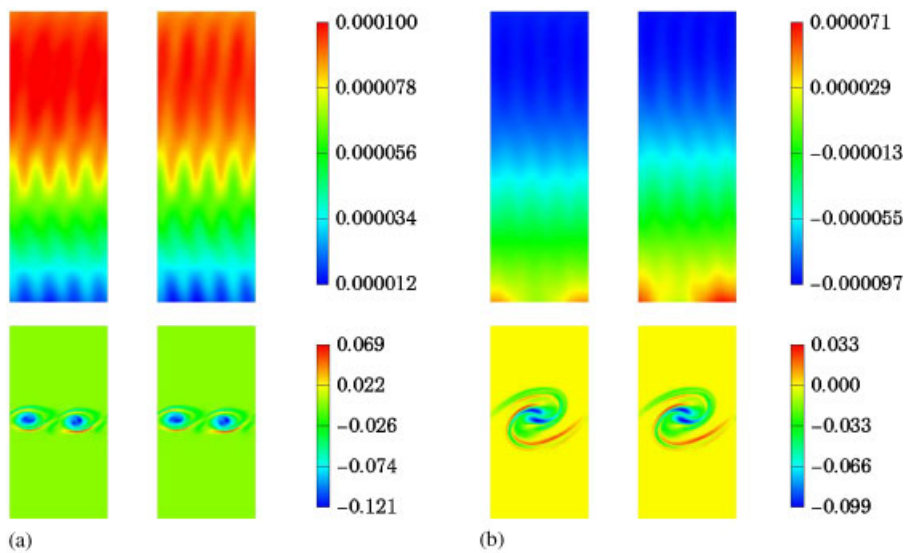

Plate 2. Non-isothermal case. Instantaneous fields at: (a) $t = 75.6$, (b) $t = 155.6$ for $M = 0.2$. Top: Instantaneous acoustic density fields in the acoustic region. Bottom: Instantaneous vorticity fields in the source region. Compressible simulation is at the left.

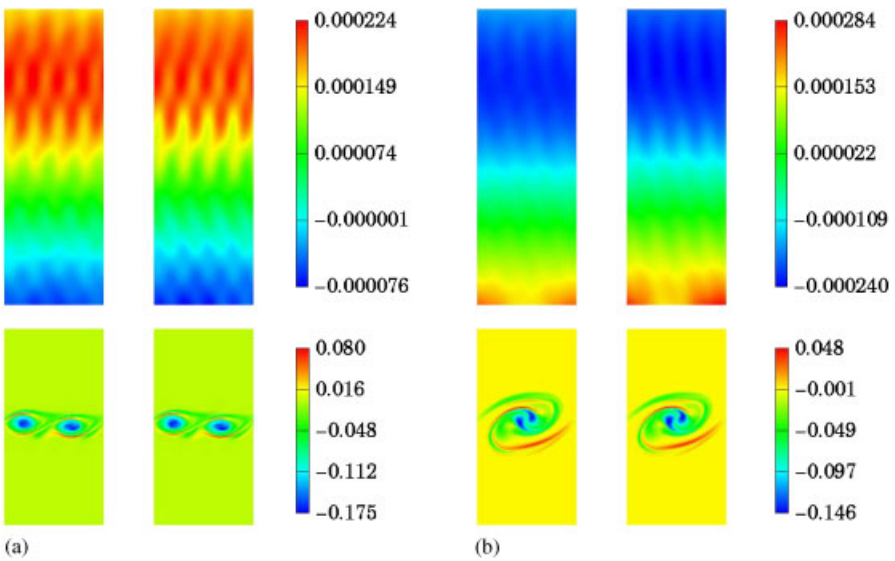

Plate 3. Non-isothermal case. Instantaneous fields at: (a) $t = 75.9$, (b) $t = 155.4$ for $M = 0.3$. Top: Instantaneous acoustic density fields in the acoustic region. Bottom: Instantaneous vorticity fields in the source region. Compressible simulation is at the left.

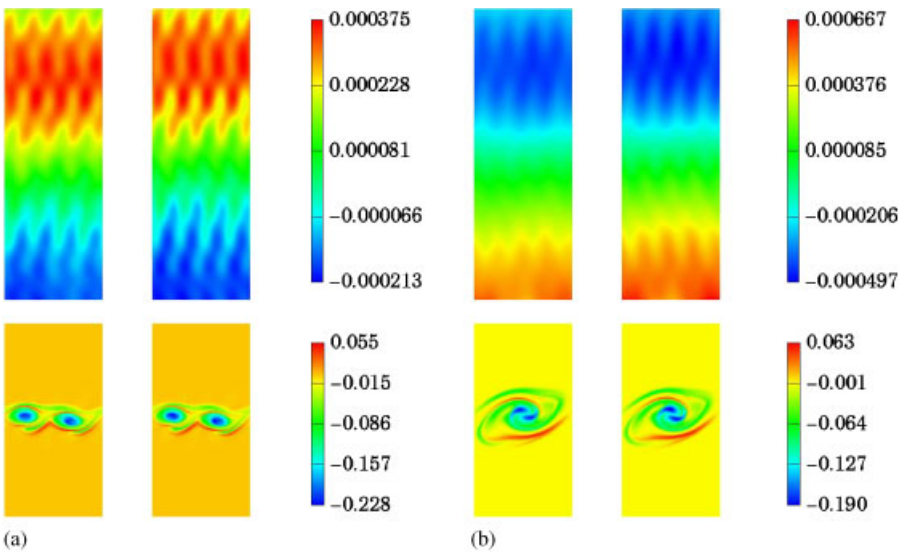

Plate 4. Non-isothermal case. Instantaneous fields at: (a) $t = 76.2$, (b) $t = 157.2$ for $M = 0.4$. Top: Instantaneous acoustic density fields in the acoustic region. Bottom: Instantaneous vorticity fields in the source region (see Figure 3). Compressible simulation is at the left.

to several pairings. In our case, the major difference with these studies is that the temporal model does not allow such an operation. Indeed, the temporal configuration can be assimilated to an approximation of the spatial model where the flow is observed in a moving window which follows the large eddies of the flow. According to References [28, 29], the speed of these eddies can be estimated by $U_c = (c_1 U_2 + c_2 U_1)/(c_1 + c_2)$ (where c_1 and c_2 are the speeds of sound in the regions of densities ρ_1 and ρ_2). Then, the frame associated with the temporal description translates at a uniform speed in the streamwise direction with respect to the frame associated with the spatial model. Finally, by this translation, the ensemble-average of any flow quantity can be expressed by means of an average operator over the streamwise direction at each instant of the temporal evolution of the flow. In this way, the dynamic quantity is averaged over a smaller number of pairings than in References [5, 7], which is balanced by the deterministic nature of this test case. To resume the mean flow treatment, the LEE are considered for the perturbation $(\rho^{(1)}, p^{(1)}, u_i^{(1)})$ over the mean flow (ρ_0, p_0, u_{0i}), with

$$\rho_0(y,t) = \langle \rho^{(0)} \rangle (y,t)$$
$$p_0(y,t) = \langle p^{(0)} \rangle (y,t)$$
$$u_{0i}(y,t) = \langle u_i^{(0)} \rangle (y,t)$$

4.4. Parameters

As the isothermal and non-isothermal tests have some common features, their computational parameters will be described in the same part of the paper. The geometries of the physical and computational domains are shown in Figure 2.

The centre of the mixing layer is chosen to be located at $y^* = 0$. In order to reduce the computational time of the compressible DNS and LEE simulations, while keeping a propagation zone as large as possible in the y-direction, the physical domain is not centred on the mixing layer. The physical domain extends from $y^* = -30\delta_\omega^*$ to $y^* = 120\delta_\omega^*$ in these simulations. The incompressible and LMNA simulations do not need to have a physical domain as large as the compressible DNS and the LEE. Their domain can be limited to the source region only. Then the physical domain extends from $y^* = -30\delta_\omega^*$ to $y^* = 30\delta_\omega^*$ in the incompressible and LMNA simulations. In the streamwise direction, the situation is more simple: all physical domains are identical. So for each simulation the domain extends from $x^* = 0$ to $x^* = 30.7\delta_\omega^*$ in the streamwise direction.

In the compressible and LMNA simulations, the grid resolution is imposed by the small scales of the flow. They have exactly the same spatial resolution in the two directions. The number of grid points are 256×501 for the incompressible and LMNA simulations, whereas there are 256×1251 points for the compressible simulation.

The grid resolution of the LEE simulation is chosen to be half that of the DNS. Actually, only every second point of the CFD grid is kept for the acoustic resolution. The use of CFD data in the LEE code need not therefore introduce spatial interpolations. There are 128×626 grid points for the LEE resolution.

The isothermal case corresponds to the ratio $T_1^*/T_2^* = 1$, and the non-isothermal one corresponds to $T_1^*/T_2^* = 2$.

5. RESULTS AND DISCUSSION

5.1. Isothermal case

The temporal configuration of a mixing layer in the isothermal case is treated in this first application in order to confirm that it is a good choice for validation of a hybrid method. In this case, the LMNA equations are equivalent to the conventional incompressible Navier–Stokes equations, and as discussed in Section 3, the source term (25) is consistent, in the isothermal case, with that defined in Reference [5], which is finally used in this part.

The scheme in Figure 3 shows that the studied domain is divided in two separated zones. The region of space located at the bottom (for $-L_y/2 \leqslant y \leqslant L_y/2$) is considered as a sound production zone. This region corresponds exactly to the computational domain of the LMNA. It is the region where the acoustic sources are defined. The zone situated at the top (for $L_y/2 \leqslant y \leqslant L'_y$) is called the acoustic propagation zone. In this region, the acoustic sources are supposed to be negligible. In fact, they are taken to be zero in the case of the hybrid method (the sources being computed in the LMNA domain presented in Figure 2). To qualify the hybrid method results, the density fields are compared to the compressible DNS results in the acoustic zone.

The common parameters of the isothermal test are those defined in the previous part. The Mach number is $M = 0.2$ (M being defined by $M = U^*_{\text{ref}}/\sqrt{\gamma r^* T^*_{\text{ref}}}$ where $U^*_{\text{ref}} = U^*_1 - U^*_2$ and $T^*_{\text{ref}} = T^*_2$). The non-dimensional time scale presented in the following results is related to the non-dimensional time used in the compressible simulations ($t^*_{\text{ref}} = \delta^*_\omega/\sqrt{\gamma r^* T^*_{\text{ref}}}$), which requires a rescaling of the LMNA results (based on $t^*_{\text{ref}} = \delta^*_\omega/U^*_{\text{ref}}$). The non-dimensional time steps are $\mathrm{d}t_{\text{comp}} = 0.0125$, $\mathrm{d}t_{\text{LEE}} = 4 \times \mathrm{d}t_{\text{comp}}$ and $\mathrm{d}t_{\text{LMNA}} = 10 \times \mathrm{d}t_{\text{comp}}$.

Plate 1 shows the results provided by the hybrid method and by the compressible DNS for two different instants of the evolution.

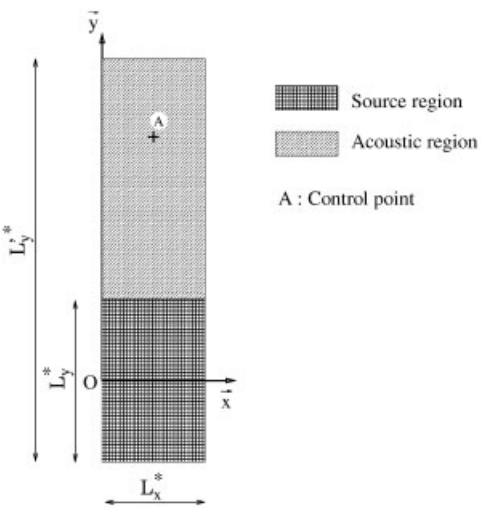

Figure 3. Localisation of the acoustic and the source regions.

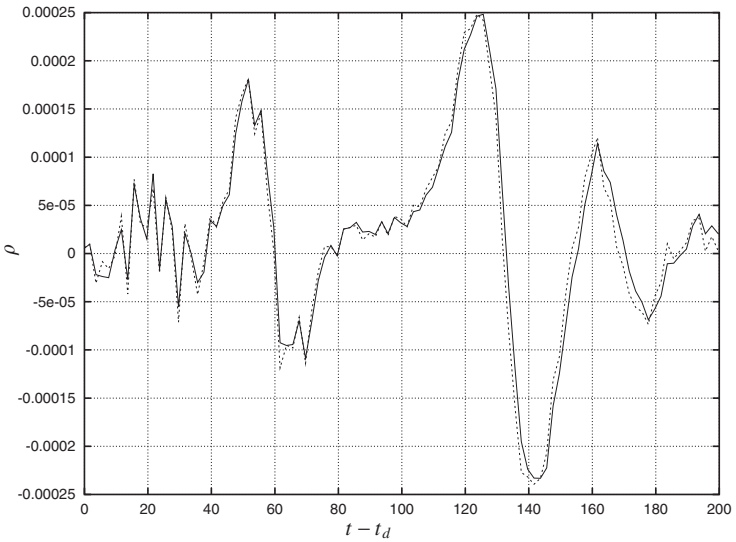

Figure 4. Isothermal case. Time history of the acoustic density for $M = 0.2$ at the point A ($x = 15.35$, $y = 101.76$). — Compressible DNS; - - - Hybrid method.

Very good agreement can be seen in the vorticity, and density fields at the beginning of the solution ($t = 53.6$, Plate 1(a)). Qualitatively, the vorticity field seems to follow the same dynamic in the two approaches in Plate 1(b), but visibly, some temporal shift exists when looking at the density fields in the propagation zone after a long calculation time. To look more precisely at what is happening, Figure 4 shows the evolution of the acoustic density at a given point A (see Figure 3) of co-ordinates ($x = 15.35, y = 101.76$) with respect to the retarded time. The use of the retarded time allows a direct comparison between the events that occur in the mixing layer and the acoustic consequences at the point A. The agreement between the two curves is good. Nevertheless, we can observe a temporal gap for t_r greater than about 100. This gap is also well visible in Figure 5 when looking at the evolution of the mean acoustic density over the streamwise direction at $y = 101.76$.

In fact, the difference is produced by the delay of the LMNA simulation with regard to the compressible simulation. This delay appears clearly in Figure 6 for the time evolution of the vorticity ($\omega = \partial v/\partial x - \partial u/\partial y$) in the middle of the mixing layer (at the co-ordinates $x = 15.35, y = 0$). This figure shows also a temporal gap between the dynamic evolutions of the compressible and the LMNA computations for t greater than about 120. The source terms being computed using the data of the LMNA, it is obvious that a temporal gap between the dynamic features induces the same temporal gap in the acoustic results. This temporal advance of the incompressible simulation with regard to the compressible one can be explained by the stabilizing effects of the compressibility.

To conclude the discussion about these first results, it appears that the temporal configuration is able to provide an appropriate test case in a validation step of aeroacoustic hybrid approach.

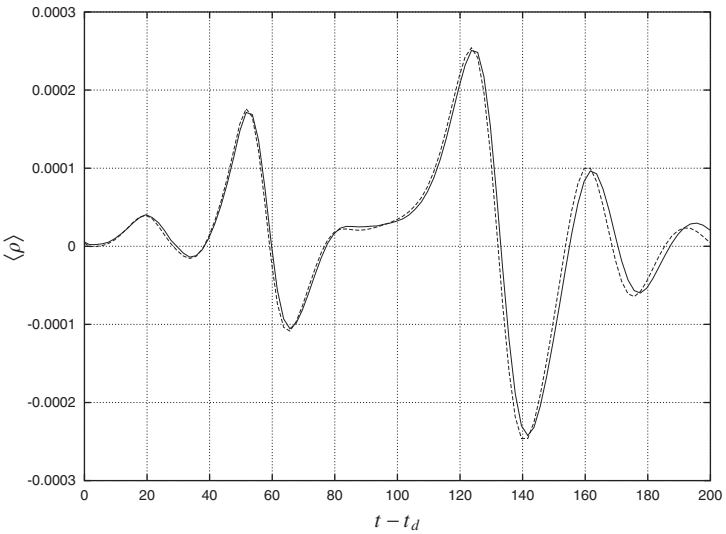

Figure 5. Isothermal case. Time history of the mean acoustic density over the streamwise direction for $M = 0.2$ at $y = 101.76$. — Compressible DNS; - - - Hybrid method.

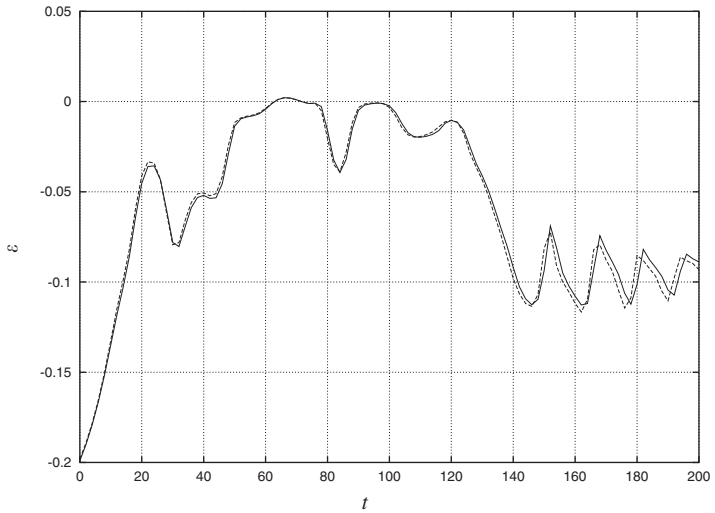

Figure 6. Isothermal case. Time history of the vorticity for $M = 0.2$ in the middle of the mixing layer ($x = 15.35,\ y = 0$). — Compressible DNS; - - - LMNA solution.

5.2. *Non-isothermal case*

The temporal configuration of a non-isothermal mixing layer is now studied. The initial temperature field is now defined by the Crocco-Buseman relation where $T_1 = 2T_2$ (Section 4.1). The complete acoustic source expression obtained from Equation (26) is employed in the

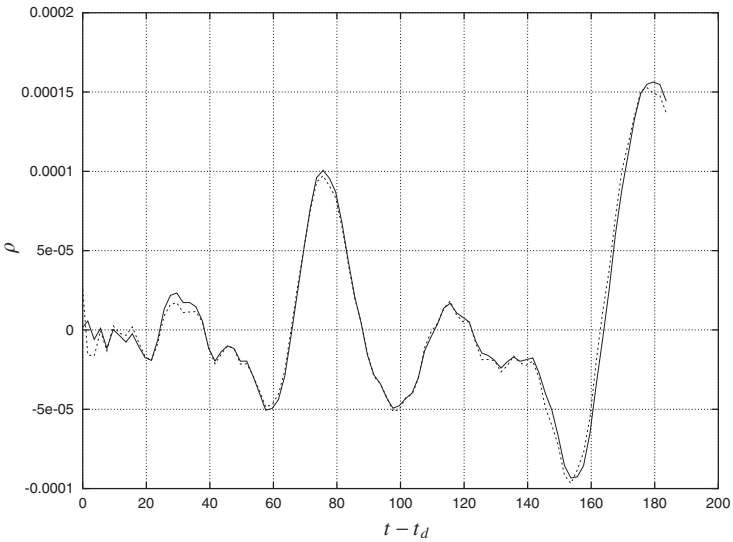

Figure 7. Non-isothermal case. Time history of the acoustic density for $M = 0.2$ at the point A ($x = 15.35$, $y = 101.76$). — Compressible DNS; - - - Hybrid method.

hybrid code. A first simulation is computed with $M = 0.2$ to validate the source term's formulation. Results are presented in Plate 2 and Figure 7. Comparisons of the compressible DNS and the hybrid method show as good an agreement as in the isothermal test. The acoustic source definition is well compatible with the LMNA simulation and restores adequately the waves emitted by a non-isothermal mixing layer. As suggested in the presentation of the LMNA equations, the Mach number does not appear in this set of equations. In fact, the low Mach number approximation used here can be considered an incompressible system in which the effects of temperature variations on the dynamic evolution are retained. Then, when the following denomination 'LMNA simulation at $M = 0.2$' is used, the exact denomination should be 'LMNA simulation corresponding to a $M = 0.2$ compressible simulation'. An interesting consequence of this point is that a single LMNA simulation can provide results comparable to compressible simulations at different Mach numbers with the aid of a simple rescaling of the velocity fields and the temporal reference. The limit of this point is the limit of the incompressible assumption, and the agreement between the two methods will decrease with increase of the Mach number.

Two other acoustic simulations are performed with $M = 0.3$ and 0.4 in order to explore the limit of the present hybrid method in terms of Mach number range. The time steps of the different simulations can be found in Table I. Only one LMNA simulation of the flow has been computed: the given time steps in this case are just used for renormalisation of the flow dynamic corresponding to different Mach numbers. The choice of different LEE simulation time steps has been motivated so as to obtain coincident instants in compressible and hybrid solutions for best comparison. The other parameters are unchanged with regard to the previous simulations. Acoustic and dynamic fields are shown in Plates 3 and 4, respectively, for $M = 0.3$ and 0.4 and the time history of the acoustic density is given for a chosen point in Figures 8 and 9.

Table I. Time steps of the non-isothermal simulations.

M	$\mathrm{d}t_{\mathrm{comp.}}$	$\mathrm{d}t_{\mathrm{LMNA}}$	$\mathrm{d}t_{\mathrm{LEE}}$
0.2	0.0125	0.125	0.05
0.3	0.01875	0.1875	0.0625
0.4	0.025	0.25	0.0625

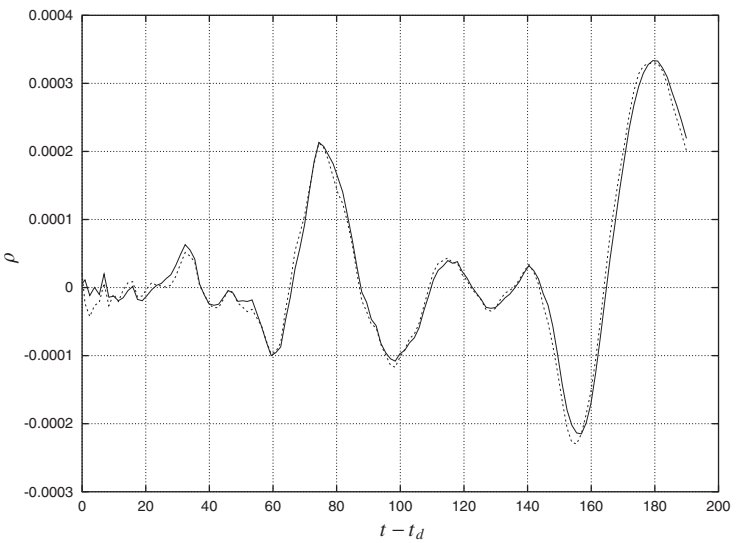

Figure 8. Non-isothermal case. Time history of the acoustic density for $M = 0.3$ at the point A ($x = 15.35$, $y = 101.76$). — Compressible DNS; - - - Hybrid method.

These results show good agreement with the compressible results. Nevertheless, the expected behavior with the increasing Mach number seems verified: the temporal gap increases with the Mach number. This gap is clearly identified in Figures 10, 11 and 12 where it appears for t_{r} greater than about 120 at $M = 0.2$ (which is comparable to the isothermal case), whereas it appears earlier as M increases ($t_{\mathrm{r}} \geqslant 60$ for $M = 0.3$ and $t_{\mathrm{r}} \geqslant 40$ for $M = 0.4$).

However, it is worth noting that the amplitudes stay very close to those given by the compressible simulation, even at $M = 0.4$.

Lastly, Figure 13 shows the mean absolute error between the hybrid method and the compressible DNS for the non-isothermal simulations. The error is defined by the relation

$$\varepsilon_\rho(t - t_{\mathrm{d}}) = \frac{1}{S} \int\int_S |\rho_{\mathrm{LEE}} - (\rho_{\mathrm{comp.}} - \rho_1)| \, \mathrm{d}S \tag{35}$$

where S is the area of the acoustic region, and t_{d} is the time needed for an acoustic wave to leave the domain.

This figure confirms that the quality of the hybrid approach based on the LMNA decreases whereas the Mach number increases. Moreover, the error increases strongly (it is particularly

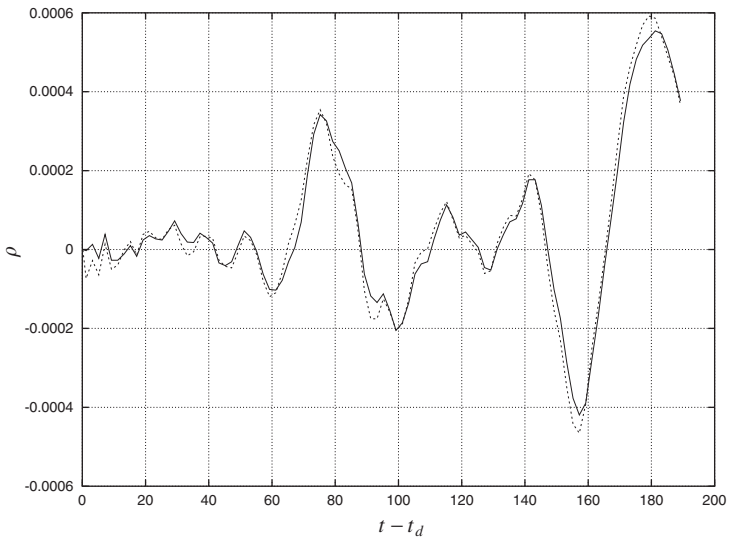

Figure 9. Non-isothermal case. Time history of the acoustic density for $M = 0.4$ at the point A ($x = 15.35$, $y = 101.76$). — Compressible DNS; - - - Hybrid method.

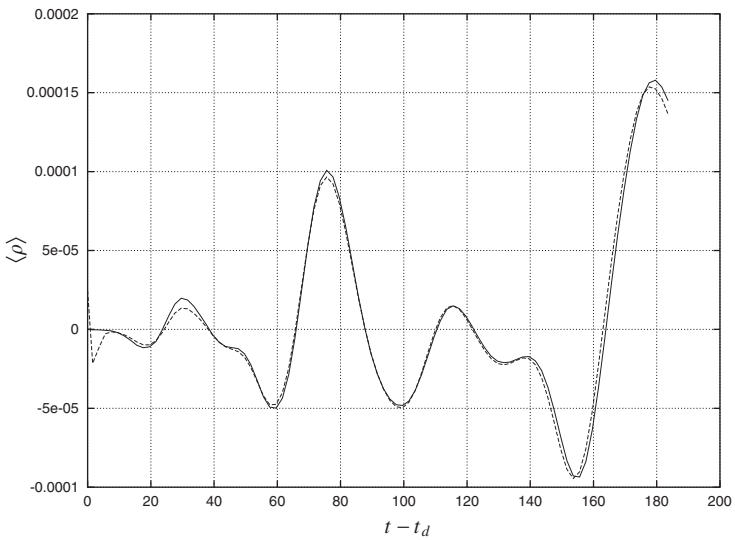

Figure 10. Non-isothermal case. Time history of the mean acoustic density over x at $y = 101.76$ for $M = 0.2$. — Compressible DNS; - - - Hybrid method.

visible on the $M = 0.2$ simulation) when the temporal gap becomes visible. Indeed, the error defined by (35) then compares fields which should appear at staggered instants, automatically inducing an increase of the error. However, in the three cases, the error hardly reaches 10% of the maximum value of the acoustic density along the whole simulation.

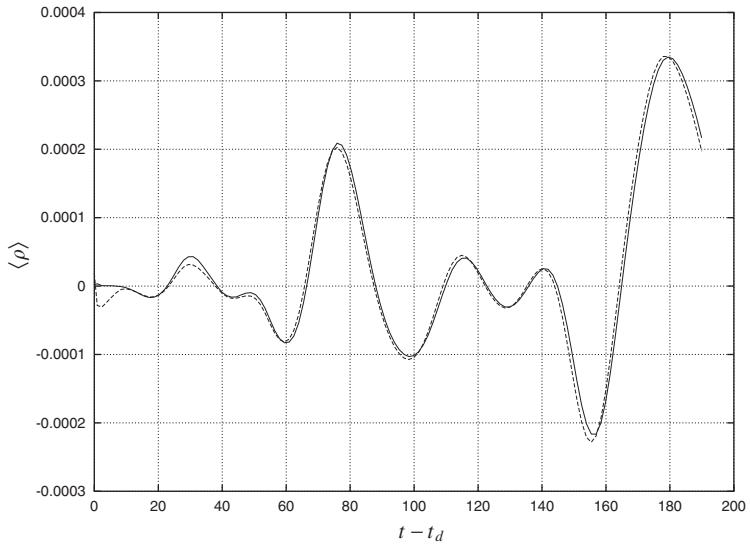

Figure 11. Non-isothermal case. Time history of the mean acoustic density over x at $y = 101.76$ for $M = 0.3$. — Compressible DNS; - - - Hybrid method.

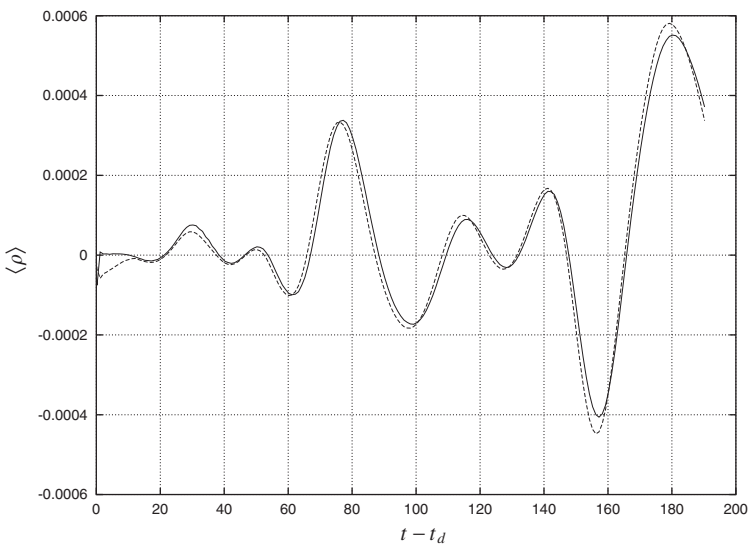

Figure 12. Non-isothermal case. Time history of the mean acoustic density over x at $y = 101.76$ for $M = 0.4$. — Compressible DNS; - - - Hybrid method.

To complete this discussion, it is interesting to compare the simulation times of each method. The three compressible simulations[‡] required 120 h of calculation for the $M = 0.2$

[‡]On a Xeon PIII processor, 700 MHz CPU clock, 1 Mo L_2 cache.

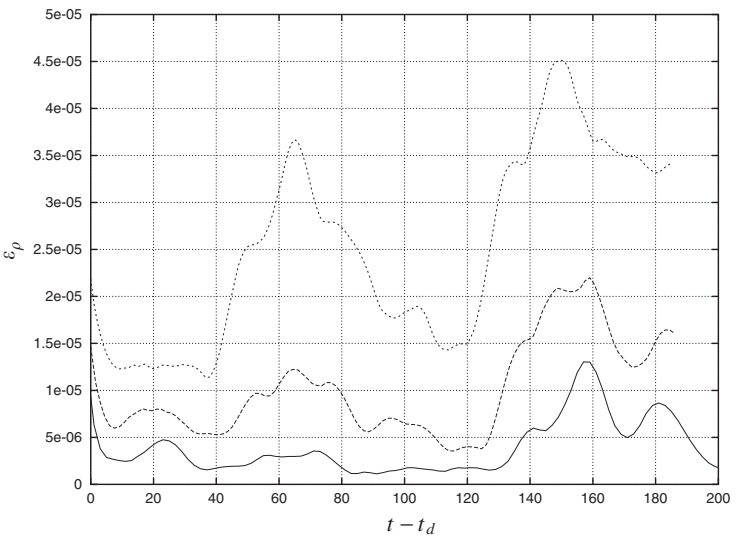

Figure 13. Non-isothermal case. Time history of the mean error on acoustic density for simulations corresponding to the three different Mach numbers. — $M = 0.2$; - - - $M = 0.3$; $\cdots$ $M = 0.4$.

case, 80 h for $M = 0.3$ and 60 h for $M = 0.4$. On the other hand, the LMNA computation (see footnote ‡) was about 14 h long, and the LEE simulation[§] times were about 7, 4.5 and 3.5 h for M equal to 0.2, 0.3 and 0.4, respectively. The hybrid method does not then provide a decisive advantage when the flow reaches Mach numbers greater than 0.4. This however is not a major drawback since hybrid methods are mainly attractive for small Mach numbers. On the contrary, the proposed hybrid technique produces an undeniable gain when computing flows evolving at very low Mach number, and particularly when a parametric study based on the Mach number is considered. Indeed, the cost of the whole non-isothermal case of the present study is approximately 270 h in the compressible simulation, whereas the hybrid method required 29 h only (the LMNA simulation being computed only once for the whole study).

6. CONCLUSION

This paper presents a hybrid aeroacoustic approach for non-isothermal flows composed of a low Mach number approximate (LMNA) fluid dynamic simulation and a linearized Euler equation (LEE) based propagation code.

The LMNA eliminates compressibility effects but preserves inhomogeneities related to temperature gradients. Compatible acoustic source terms for the LEE are determined analytically. A simple rescaling of the dynamic simulation allows the acoustics of a relatively wide range of subsonic flows to be studied.

[§]On a Athlon processor, 900 MHz CPU clock, 256 Ko L_2 cache.

Numerical tests are performed on a temporal non-isothermal mixing layer flow and compared to compressible Direct Numerical Simulations. Results show very good agreement for a Mach number of 0.2 and remain valid for relatively high subsonic Mach number, up to $M = 0.4$.

REFERENCES

1. Lighthill MJ. On sound generated aerodynamically I General theory. *Proceedings of the Royal Society of London, Series A* 1952; **211**:567–587.
2. Lighthill MJ. On sound generated aerodynamically II Turbulence as a source of sound. *Proceedings of the Royal Society of London, Series A* 1954; **223**:1–32.
3. Phillips OM. On the generation of sound by supersonic turbulent shear layer. *Journal of Fluid Mechanics* 1960; **9**(1):1–28.
4. Lilley GM. The generation and radiation of supersonic jet noise. Vol. IV: Theory of turbulence generated jet noise, noise radiation from upstream sources and combustion noise. *AFAPL report*, vol. 53, 1972.
5. Bailly C, Bogey C, Juvé D. Computation of flow noise using source terms in linearized Euler's equations. *AIAA paper 00-2047*, 2000.
6. Ewert R, Meinke M, Schröder W. Comparison of source term formulations for a hybrid CFD/CAA method. *AIAA paper 01-2200*, 2001.
7. Bogey C, Bailly C, Juvé D. Computation of flow noise using source terms in linearized Euler's equations. *AIAA Journal* 2002; **40**(2):235–243.
8. Béchara W, Bailly C, Lafon P, Candel S. Stochastic approach to noise modeling for free turbulent flows. *AIAA Journal* 1994; **32**(3):455–463.
9. Blom CPA, Verhaar BT, van der Heijden JC, Soermarwoto BI. A linearized Euler method based prediction of turbulence induced noise using time-averaged flow properties. *AIAA paper 01-1100*, 2001.
10. Freund JB, Lele SK, Moin P. Matching of near/far-field equation sets for direct computation of aerodynamic sound. *AIAA paper 93-4326*, 1993.
11. McMurtry PA, Jou W-H, Riley JJ, Metcalfe RW. Direct numerical simulations of a reacting mixing layer with chemical heat release. *AIAA Journal* 1986; **24**(6):962–970.
12. Cook AW, Riley JJ. Direct numerical simulation of a turbulent reactive plume on a parallel computer. *Journal of Computational Physics* 1996; **129**:263–283.
13. de Charentenay J, Thévenin D, Zamuner B. Comparison of direct numerical simulations of turbulent flames using compressible low-Mach number formulations. *International Journal for Numerical Methods in Fluids* 2002; **39**:497–515.
14. Hardin JC, Pope DS. An acoustic/viscous splitting technique for computational aeroacoustics. *Theoretical and Computational Fluid Dynamics* 1994; **6**:323–340.
15. Djambazov GS, Lai C-H, Pericleous KA, Wang Z-K. A coarse grid extraction of sound signals for computational aeroacoustics. *International Journal for Numerical Methods in Fluids* 2002; **40**:1515–1525.
16. Munz C-D, Roller S, Klein R, Geratz KJ. The extension of incompressible flow solvers to the weakly compressible regime. *Computational Fluids* 2003; **32**:173–196.
17. Strahle WC. Noise production by fluid inhomogeneities. *AIAA Journal* 1976; **14**(7):985–987.
18. Comte P, Lesieur M, Lamballais E. Large- and small-scale stirring of vorticity and a passive scalar in 3-D temporal mixing layer. *Physics of Fluids A* 1992; **4**(12):2761–2778.
19. Vreman B, Geurts B, Kuerten H. Large-eddy simulation of the temporal mixing layer using the Clark model. *Theoretical and Computational Fluid Dynamics* 1996; **8**:309–324.
20. Vreman B, Geurts B, Kuerten H. Comparison of numerical schemes in large-eddy simulation of the temporal mixing layer. *International Journal for Numerical Methods in Fluids* 1996; **22**:297–311.
21. Fortuné V, Lamballais E, Gervais Y. Etude par simulation numérique directe temporelle des effets de la température sur l'émission acoustique des couches de mélange. *Comptes Rendus de l'Academie des Sciences* 2000; **328**:693–700.
22. Lele SK, Ho CM. Acoustic radiation from temporally evolving free shear layers. *Technical report*, Stanford University, 1994.
23. Whitemire J, Sarkar S. Validation of acoustic-analogy predictions for sound radiated by turbulence. *Physics of Fluids* 2000; **12**(2):381–391.
24. Lele SK. Compact finite difference scheme with spectral-like resolution. *Journal of Computational Physics* 1992; **103**:16–42.
25. Golanski F, Fortuné V, Lamballais E. Prediction of noise radiated by a non-isothermal mixing layer using a low Mach number approximation. In *RTO AVT Symposium on aging mechanisms and control: Part A—Developments in computational Aero- and Hydro-acoustics*, Manchester, UK, RTO-MP-079(I), 2001.

26. Giles MB. Nonreflecting boundary conditions for Euler equation calculations. *AIAA Journal* 1989; **28**(12):2050–2058.
27. Press WA, Flannery BP, Teukolsky SA, Vetterling WT. *Numerical Recipes*. Cambridge University Press: Cambridge, 1989.
28. Bogdanoff DW. Compressibility effects in turbulent shear layers. *AIAA Journal* 1983; **21**(6):926–927.
29. Papamoschou D, Roshko A. The compressible turbulent shear layer: an experimental study. *Journal of Fluid Mechanics* 1988; **197**:453–477.

